Optical and Microphysical Characterization of Atmospheric Aerosol in the Central Mediterranean during Simultaneous Volcanic Ash and Desert Dust Transport Events

Alessia Sannino[1], Salvatore Amoruso[1], Riccardo Damiano[1], Simona Scollo[2], Pasquale Sellitto[3], Antonella Boselli[4, *]

[1] Dipartimento di Fisica "Ettore Pancini", Complesso Universitario di Monte S. Angelo, Via Cintia, I-80126 Napoli (Italy).
[2]Istituto Nazionale di Geofisica e Vulcanologia, Osservatorio Etneo, Piazza Roma 2, 95125 Catania, Italy.
[3]Univ. Paris Est Créteil and Université de Paris, CNRS, Laboratoire Interuniversitaire des Systèmes Atmosphériques, Institut Pierre Simon Laplace, Créteil, France.
[4]Consiglio Nazionale delle Ricerche Istituto di Metodologie per l'Analisi Ambientale, C.da S. Loja, 85050 Tito Scalo, Potenza Italy.

***Corresponding author:**
Dr. Antonella Boselli
boselli@imaa.cnr.it

Keywords: Remote Sensing, Volcanic Aerosol, Saharan Dust, Aerosol Size Distribution.

Abstract:
Volcanic plume aerosol following the paroxysmal event of Mount Etna in February 21st - 26th, 2021 was detected in Naples area (Italy), together with transport of Saharan dust aerosol, combining lidar, sunphotometer and satellite observations with back-trajectories and dispersion models simulations. Lidar data allowed to clearly distinguish the two main aerosol components, to investigate the spectral dependence of the aerosol optical properties and to retrieve their microphysical properties, essential for a detailed aerosol characterization. A new Monte Carlo algorithm, capable of retrieving the particle size distribution from lidar measurements, was applied. Lidar results are in good agreement with columnar integrated sunphotometer data. This combination of novel lidar observations of the vertically-resolved aerosol microphysics, column observations and modelling allows for a more complete description of multi-layered aerosol conditions.

1. Introduction

Atmospheric aerosol is of particular interest for its impact on the climate system, air quality and human health, to mention a few (Ghan et al., 2012; Zhang et al., 2012; Mallet et al., 2019; Zhang, 2020). Nevertheless, aerosol studies are generally subject to large uncertainties due to the great temporal and spatial variability of sources, distribution and composition.
As a specific example, the spatiotemporal characterization of load and properties of the aerosol layer over the Central Mediterranean area is very complex due to the coexistence of particles of different nature and typology, produced by local sources or long-range transport phenomena (Lelieveld et al., 2002; Xu et al., 2020). Larger coarse-mode aerosol originates mainly from natural sources and includes mineral dust from African deserts (e.g. Pisani et al., 2011; Valenzuela et al., 2014; Soupiona et al., 2020) as well as marine aerosol from Mediterranean Sea and Atlantic Ocean (e.g. Di Iorio et al., 2009; Khedidji et al., 2020). Conversely, fine polluted aerosol derives from

local anthropogenic activities or long range transport from continental Europe (e.g. Hatzianastassiou et al., 2009; Perrone et al., 2013) and Asia (Lelieveld et al., 2002). Biomass burning aerosol is also frequently observed, mainly in summertime, due to favourable, hot and dry conditions of the Mediterranean area; both local (Pace et al., 2005; Perrone and Burlizzi, 2016; Boselli et al., 2021) and long range transported (from Europe and North America) fire particles contribute to such kind of aerosol (e.g. Baars et al., 2019; Papanikolaou et al., 2020). Finally, the Mediterranean area hosts numerous active volcanoes, like Mount Etna and Stromboli, and fumaroles, such as those in Aeolian Islands and Phlegraean Fields.

Volcanic eruptions represent an extraordinary opportunity for the progress of the volcanic science and near real time observations of these events are very important for a deeper understanding of their effects on climate and life. In this respect, in the last decade numerous environmental studies were carried out worldwide to assess the impact of major volcanic eruptions on the atmosphere (e.g. Eyjafjallajökull in 2010; Nabro in 2011, Calbuco in 2015; Raikoke in 2019; Cumbre Vieja in 2021) . These studies were carried out using ground-based and air-borne remote sensing instruments (lidar, photometer), satellite observations and model results (e.g. Mattis et al., 2010; Papayannis et al., 2011; Sawamura et al., 2012; Mona 2012; Pappalardo et al., 2013; Noh et al., 2017; Lopes et al., 2019; Bègue et al., 2020; Klekociuk et al., 2020; Vaugan et al., 2021). They mainly refer to long-range transport events and aim at tracking the amounts of aerosol and SO_2 injected in the atmosphere by means of continuous observations of their spatial distribution and temporal evolution.

In the Mediterranean area, Mount Etna's emissions impact the atmospheric aerosol content and properties with both its continuous passive degassing (Sulpizio et al., 2014; Sellitto et al., 2020) and mild- to high-intensity explosive activity (Thomas et al., 2005; Sellitto at al., 2016), whose effects systematically influence an area of several hundred km downwind its degassing craters (Sellitto et al., 2017). Therefore, the Mediterranean basin provides a perfect natural laboratory to characterize different aerosol types whose transport is marked by aging and mixing phenomena favoured by high evaporation, low precipitation and remarkable solar activity (Michaelides et al., 2018). The coexistence of different aerosol types makes particularly challenging their differentiation. Nevertheless, this is necessary for the study of the inherent physico-chemical processes and can be realised through the analysis of the observed properties of the aerosol layer. The investigation of aerosol properties during specific advection events is crucial.

Here we report on the observation of aerosol optical and microphysical properties in the central Mediterranean region, at the Naples station, during a period characterised by both a major Saharan dust outbreak and a major eruption of Mount Etna with an uncommon transport towards the north (Sellitto et al., 2021). This exceptional event is here characterised by combining range resolved lidar measurements, columnar integrated sunphotometer data and air-mass back trajectories, as well as satellite data and dispersion models outcomes. Strikingly, the application of a novel inversion algorithm to real lidar data demonstrates how a clear classification of the aerosol layers can be gained for multilayered atmospheric conditions through the retrieved size distributions providing a remarkable feature of the proposed approach towards a more reliable characterization of the atmospheric event.

2. Material and methods

The observation station at University of Naples "Federico II" is part of ACTRIS (Aerosol, Clouds and Trace Gases Research Infrastructure) (Pappalardo, 2018) a pan-European research infrastructure providing high quality scientific results on atmospheric aerosols, clouds, and trace gases. The station is equipped with ground-based passive and active remote sensing instruments and near surface devices for the measurement of atmospheric aerosol geometrical, optical and microphysical properties.

The station (southern Italy, 40.838° N, 14.183° E, 118 m above sea level) is located in the Mediterranean basin, an area periodically affected by long-range transport of anthropogenic and natural aerosols. The former arises from industrialized areas in Europe, whereas the latter is mainly due to volcanic eruptions, forest fires and very frequent Saharan dust outbreaks (Pisani et al., 2011).

2.1 Aerosol profiling using lidar observations

The station is provided with a multiwavelength lidar system operating since year 2000 in the frame of the EARLINET (European Aerosol Lidar NETwork) European network of advanced lidar station (Pappalardo et al., 2014) aiming at measuring the horizontal, vertical, and temporal distribution of aerosols on a continental scale. The lidar transmitter is a Nd:YAG laser providing beams at wavelengths of 1064 nm, 532 nm and 355 nm with energies of 0.65, 0.15 and 0.1 J, respectively, at a repetition rate of 20 Hz. The receiver consists of a Newtonian telescope with a diameter of 30 cm and a focal length of 120 cm. The spectral selection unit allows detecting elastic signals at 1064 nm, 532 nm (parallel and cross-polarized signals) and 355 nm, as well as Raman echoes at 386 nm (N_2), 607 nm (N_2) and 407 nm (H_2O). Raw data are typically acquired with 1-minute temporal resolution and 15 m spatial resolution.

Lidar-derived aerosol properties have been investigated in term of vertical profiles of aerosol backscattering ($\beta(z)$) at 355 nm, 532 nm and 1064 nm, and extinction ($\alpha(z)$) at 355 nm and 532 nm, as well as aerosol depolarization ratio ($\delta(z)$) at 532 nm.

The profiles $\beta(z)$ were retrieved from nocturnal and diurnal lidar observations using the Klett–Fernald algorithm (Klett, 1981; Fernald. 1984) and the Raman method (Ansmann et al., 1992), respectively. The profiles $\alpha(z)$ are measured during nighttime following the procedure introduced by Ansmann et al. (1990). The used algorithms comply with EARLINET quality-assurance requirements detailed in Pappalardo et al., (2004) and Böckmann et al., (2004).

Simultaneous elastic and Raman lidar measurements allow to obtain independent estimations of $\beta(z)$ and $\alpha(z)$ profiles. This, in turns, allows the estimation of the extinction-to-backscatter ratio, the so-called Lidar Ratio (LR). Moreover, calibrated $\delta(z)$ profiles are retrieved from the backscattered light components polarized along the directions parallel and perpendicular to the plane of linear polarization of the transmitted laser beam at 532 nm, following the inversion procedure reported by Biele et al., (2000) and Freudenthaler et al., (2009). The LR and δ are key parameters to classify aerosol typology because both depend on specific aerosol properties (shape, composition).

The lidar configuration with three backscatter and two extinction wavelengths ($3\beta + 2\alpha$) allows studying the spectral dependence of the atmospheric aerosol optical properties and retrieving aerosol microphysical parameters according to state of the art procedures (Müller et al., 1999; Böckmann et al., 2005; Burton et al., 2016; Chemyakin et al., 2016; Pérez-Ramírez et al., 2020; McLean et al., 2021), thus gaining a complete aerosol characterization.

Using lidar measurements of $\beta(z)$ and $\alpha(z)$ at λ_1=355nm and λ_2=532 nm, the Angstrom Exponents for backscatter, $BAE=\log(\beta_1/\beta_2)/\log(\lambda_2/\lambda_1)$, and extinction, $EAE= \log(\alpha_1/\alpha_2)/\log(\lambda_2/\lambda_1)$, have been estimated. Larger values of BAE and EAE can be linked to a prevalence of smaller aerosol particles and vice-versa, which also contribute to the aerosol type characterization (Liua et al., 2001).

Moreover, following the method reported by Sorrentino et al. (2021), here we also retrieve the particle size distribution from lidar measured optical parameters by modeling the particle number size distribution as a superposition of log–normal distributions and using a Bayesian model and a Monte Carlo algorithm to estimate mode, width and height of each distribution. The reliability of such approach was tested in Sorrentino et al. (2021) on synthetic data generated by distributions containing one or more modes and perturbed by Gaussian noise as well as on three real datasets obtained from the AERONET database.

The size distribution analysis allows to better characterize the nature of atmospheric aerosol since accumulation and coarse mode fractions contribute in different ways for the various kind of aerosol. For example, accumulation mode particles mainly derive from anthropogenic activities and correspond to sulfate, black carbon, organic carbon, nitrates, both directly emitted (black carbon) or coming from gas-to-particle conversion. Conversely, coarse mode particles mainly originate from natural sources and correspond, in our region, to large mineral dust and sea salt aerosol (Müller at al., 2007).

2.2 Columnar aerosol properties

A ground-based dual polarization and triple mode (sun, sky, lunar) photometer (CIMEL CE318TS-M) is operative since 2016 at the University of Naples "Federico II" in the frame of AERONET (AErosol RObotic NETwork) (Holben et al, 1998), the network of globally distributed ground-based passive remote sensing instruments providing continuous observations of aerosol optical, microphysical and radiative properties. The system provides routine observations of columnar atmospheric aerosol properties, which represent key information for real time monitoring of aerosol content temporal evolution. It is important to notice, in this context, that columnar observations are associated to mixed aerosol layer, i.e. with possibly different aerosol types at different altitudes. The sun-photometer measures direct sun and sky-radiance at a number of fixed wavelengths within the UV-NIR spectrum (340, 380, 440, 500, 675, 870, 1020 and 1640 nm). Measured data are calibrated and processed with the AERONET inversion algorithms (Giles et al., 2019; Dubovik and King, 2000; Holben et al., 2001). Retrieved aerosol microphysical parameters are open access and available at the AERONET website (aeronet.gsfc.nasa.gov).

Level 2.0 cloud screened and quality assured data of columnar aerosol optical depth (AOD), Ångström exponent (γ), volume particle size distribution dV(r)/dln(r), ($\mu m^3\ \mu m^{-2}$) and Single Scattering Albedo (SSA) are analyzed, with the aim of studying the total column loading and size variability of atmospheric aerosol gaining further information on their absorption characteristics. Accuracy on retrieved product is reported in Dubovik et al. (2000).

2.3 Aerosol source regions identification

The HYbrid Single-Particle Lagrangian Integrated Trajectory (HYSPLIT) transport model provided by the U.S. National Atmospheric and Oceanic Administration (NOAA) Air Resources Laboratory (ARL) and available at the AERONET website (https://aeronet.gsfc.nasa.gov) is used to verify the source regions of the aerosol layers observed over the measurement area. Air masses back-trajectories, calculated at altitude levels from 0.5 to 8 km a.s.l., provide an assessment on aerosol long-range and local transport phenomena from different source regions over longer or shorter timescales (one to ten days).

The possible influence of Saharan Dust transport events is further assessed by means of the NMMB/BSC-Dust daily forecasts of dust concentration operated by the Barcelona Supercomputing Center (http://www.bsc.es/ess/bsc-dust-daily-forecast/) that provide a description of the horizontal distribution and temporal variability of the dust.

2.4 Volcanic plume detection and dispersion with satellite and modelling

The main volcanic plume dispersal was obtained by volcanological observations and simulations that every day are run from the Istituto Nazionale di Geofisica e Vulcanologia (INGV), Osservatorio Etneo. The simulations are one of the outputs of the VAMOS SEGURO project (http://www.vamosseguro.eu/) and are run using the PUFF model in a domain of $330 \times 300\ km^2$. Details in the modelling approach can be found in Azzopardi et al. (2013).

The dispersion of the volcanic plume associated to this event is also simulated using the Lagrangian dispersion model FLEXPART (Pisso et al., 2019), by means of the SO_2 volcanic tracer. The simulations are initialized with satellite-derived Mt Etna's SO_2 emission rates, in the period 21st - 26th February 2021, and are driven by the European Centre for Medium-Range Weather Forecasts (ECMWF) ERA-5 reanalysis data, as described by Sellitto et al., 2021.

Finally, the total column SO_2 Level 2 data product of the TROPOspheric Monitoring Instrument (TROPOMI) on board of the Copernicus Sentinel-5 Precursor satellite (Veefkind et al., 2012) are also used in this work in order to highlight the presence in the measurement area of SO_2 due to Mount Etna volcanic emission. The TROPOMI is an advanced multi-spectral passive grating

imaging spectrometer that measures the Solar light in spectral bands from the ultraviolet to shortwave infrared (270nm-2385nm) providing information on atmospheric composition for air quality and climate studies (Lakkala et al., 2020). It makes daily global observations of many atmospheric components like ozone (O_3), nitrogen dioxide (NO_2), sulfur dioxide (SO_2), carbon monoxide (CO), methane (CH_4), formaldehyde (HCHO) cloud and aerosol properties, with a spatial resolution of 5.5 × 3.5 km^2 at nadir.
The characteristic parameters obtained by both instruments and models used in this work are summarized in Table 1.

3. Results and Discussion

Continuous elastic/Raman lidar observations were carried out on February 25th from 08:29 to 16:42 UTC, allowing to follow the aerosol layer variability during Saharan dust and volcanic aerosol transport. The left panels of Figure 1 display colour maps addressing the temporal evolution of the Range Corrected lidar Signal (RCS) (panel (a)) and depolarization ratio (δ) (panel (b)). The right panels report lidar profiles of β(z), δ(z) and α(z) corresponding to the 16:12-16:42 time window. The spatial resolution is 60 m for β and δ and 120 m for α profiles.
The lidar profiles of Figure 1 clearly evidence two main aerosol layers. The lower one covers the range 0.7-3.5 km, whereas the higher one extends from 7.0 to 8.5 km. The lower layer is characterized by larger depolarization ratio with calibrated δ mean value of (24±5) % at 532 nm and mean LR of (31±2) sr at 355 nm and (38±6) sr at 532nm. The higher layer shows an aerosol depolarization ratio of (10±6) % at 532 nm and mean LR values of (77±14) sr at 355nm and (74±40) sr at 532nm. These properties suggest the presence of vertically-separated aerosol layers dominated by different aerosol types. The lower layer can be ascribed to aspherical particles and the LR values point to the Saharan dust typically observed over the measurement area (Pisani et al., 2011). The upper layer can be, instead, associated to the volcanic aerosol ejected by Mount Etna.
The sources of the aerosol layers can be ascertained by means of the NMMB/BSC-Dust forecast and HYSPLIT models outcomes as well as satellite images. Panels (a) and (b) of Fig. 2 report maps of the DREAM dust optical depth at 550 nm up to 0.4 and the HYSPLIT backward trajectories coming from African regions, respectively. Both support the presence of Saharan Dust transport phenomena over the measurement area in the period of interest. Moreover, such result is also in agreement with satellite images and with observations reported in Sellitto et al., 2021, demonstrating the presence of dust up to 4 km of altitude in the Naples area.
A high eruption column was produced in the night between 22nd and 23rd February during a lava fountain event at Mount Etna. The volcanic plume was initially dispersed toward the north-east direction as shown in the Meteosat image of Fig. 3(a) capturing the volcanic plume on 24th February (https://www.eumetsat.int/mount-etna-very-active-feb-march-202) and in the PUFF model simulation of volcanic dispersal and deposition (Fig. 3(b)) run every day at the Etna volcano observatory (https://www.ct.ingv.it/index.php/monitoraggio-e-sorveglianza/segnali-in-tempo-reale/simulazione-dispersione-ceneri-vulcaniche).
The simultaneous presence of a volcanic aerosol plume at higher altitude is evidenced by the image of volcanic SO_2 emission displayed in panel (c), as observed by TROPOMI (Sellitto et al., 2021), as well as by the FLEXPART model outputs showing the time-variability and the vertical profile, corresponding to 16:00-17:00 UTC time interval, of the SO_2 mass concentration over Naples station (averaged over a horizontal area of <50 × 50 km^2) reported in panels (d) and (e) of Fig. 3. As already addressed by Sellitto et al., 2021, FLEXPART simulations show that on February 25th the volcanic plume overpassed Naples from late morning to early evening, forming a layer at an altitude of 7-10 km with a maximum density between 15:00 and 18:00 UTC.
Consistently, the aerosol layer observed by lidar since 15:23 UTC at an altitude of 8- 9 km, then lowering at altitudes between 7 and 8.5 km after 16:00 UTC, showing a β peak values of 2.4×10^{-6} at 15:53 UTC, can be reliably ascribed to volcanic aerosols. The previous scenario is further supported

by the averaged values of BAE and EAE that resulted equal to (1.94±0.39) and (2.6±1.7), respectively, at this altitude range. Conversely, below 3000m the averaged values of BAE and EAE resulted to be (1.06±0.02) and (1.5±2.0), respectively. The values for the upper aerosol layer are characteristic of a mix of small sulfate and larger ash particles originating from eruption plumes of Mount Etna, whereas those for the lower layer are typical of the larger Saharan dust aerosol, according to the values reported in the Mediterranean region for these aerosol typologies (Pappalardo et al. 2004; Pandolfi et al., 2011; Papayannis et al., 2012; Soupiona et al., 2019). The characteristic parameters obtained by lidar measurements in each layer are summarized in Table 2.
Panels (a) and (b) of Figure 4 report the daily evolution of the Aerosol Optical Depth (AOD) and Angstrom coefficient, respectively, retrieved from the AERONET sunphotometer. The AOD shows a progressive increase during February 25th, reaching values of about 0.56 at 440nm and 0.49 at 500nm at 17:30 UTC. These values are in good agreement with the lidar observations that show values of the columnar AOD of (0.6±0.2) and (0.5±0.1) at 355nm and 532nm, respectively, at 16:40 UTC. The rise of the aerosol concentration in the atmospheric column is due to the increment of both dust component and volcanic plume advection, the contribution of the latter one gradually growing after 15:00 UTC, as highlighted by lidar measurements. However, the temporal evolution of the Angstrom exponent (see Figure 3(b)) suggests a predominance of larger particles associated to the Saharan dust fraction in the atmospheric column or a fraction of larger ash particles in the volcanic plume, as suggested by Sellitto et al., 2021. This aspect is also supported by the increment of the SSA value going from 440nm to 670nm (from 0.92±0.01 to 0.97±0.01). The SSA increase with time suggests a progressive evolution towards aged and less absorbing aerosol.
Finally, Figure 5(a) shows the volume particle size distribution obtained by sunphotometer data. The columnar size distributions are provided by AERONET in terms of the function $dV/dln(r)$ (expressed in $\mu m^3/\mu m^2$), where r is the particles radius and V the particles volume per unit of atmospheric surface. The profiles show a bimodal size distribution with both accumulation and coarse modes contributing to the total AOD.
The particles size distribution was also derived from lidar aerosol mean columnar optical properties applying our inversion algorithm (Sorrentino et al., 2021).
It is worth noticing that the lidar-based approach requires Raman measurements that are feasible only after sunset, meanwhile AERONET columnar size distributions are available only for diurnal data. Hence, the particle size distributions closest in time are compared, i.e. those obtained between 16:12 to 16:42 UTC for the lidar and at 15:26 UTC for the sun-photometer. The size distribution $dV/dln(r)$ (expressed in a.u.) obtained from lidar data for the range 700-9000 m is reported in Figure 5(b). The red profile refers to the mean value whereas the black dotted curves define the error band interval reporting the minimum and the maximum retrieved values. The lidar-derived size distribution is bimodal, in agreement with the sunphotometer findings. The peak mode radius values occur at about 0.20 and 2.16 μm for lidar and at 0.15 and 1.71 μm for sunphotometer, resulting in a relatively good agreement. The small differences between the mode radii are likely due to the different measurement times intervals associated with the possible increment of the atmospheric aerosol content at later times. In fact, the increase of the AOD values with time observed in Fig. 4(a) is well correlated with the temporal evolution of the AERONET size distribution showing a progressive rise of the fine mode component peak values in Fig. 5(a).
The fairly good agreement between the size distributions of Figs. 5(a) and 5(b) demonstrates the reliability of the lidar inversion algorithm and encourages getting further insights into the two different identified layers to untangle the two contributions to the atmospheric column. It is important to mention that the sunphotometric data do not provide vertical information for the size distribution; hence, lidar vertically-resolved size distributions are a unique and complementary source of information to characterise such complex aerosol multi-layered conditions. The lidar size distributions for the two regions 700-3500 m and 7000-8500 m are shown in panels (c) and (d) of Figure 5.

The two particles size distributions are very different. The particles size distribution for the Saharan dust plume (altitudes below 3500 m) shows a more elevated particle concentration in the coarse mode fraction, due to a larger mean size expected for the Saharan dust aerosol, accompanied by finer particles in the accumulation mode possibly related to local, urban aerosol contributions or very fine dust.

Conversely, in the size distribution linked to the volcanic plume (7.5-8.5 km) the fine particles mode is dominant. This finding is coherent with the larger Ångstrom exponents estimated for the volcanic plume layer and related to the smaller sulphate particles (e.g. Scollo et al., 2012; Sellitto at al., 2017). The smaller contribution of the coarse mode particles is possibly related to the large distance between the measurement area and the volcanic source (above 400 km) causing the deposition of larger volcanic ash particles. The retrieved size distribution is consistent with volcanic particle size distributions characterised by several authors and summarised by Mather and Pyle (2003). Moreover, it is also coherent with the results of Whitby (2017), who stated that a bimodal size distribution is a reasonable choice to describe the volcanic particles emission and formation processes: the coarse fraction (>2 µm) can be associated to the magma fragmentation leading to ash formation, as well as the erosion of particles from the walls of the volcanic conduit, whereas the fine particles in the accumulation mode (0.1 µm - 2 µm) are associated to gas-to-particle conversion processes leading mostly to the formation of liquid sulphate-containing aerosols.

Conclusions

Simultaneous advection of volcanic ash from Etna and long-range transport of desert dust in a Mediterranean area were observed on 25th February 2021 by ground-based passive and active remote sensing instruments of the Naples National Facilities of the ACTRIS research infrastructure. The observations, supported by satellite measurements, air-mass back trajectories and dispersion models results allowed to identify the two vertically-separated layers of different aerosol typologies, whose mean aerosol optical and microphysical properties were then addressed.

Lidar derived optical properties showed the presence of two vertically-separated aerosol layers dominated by different aerosol types. As for the first layer, the findings indicate values typical of larger and more depolarizing Saharan dust aerosol, whereas the values corresponding to the second layer are characteristic of a mix of small sulfate and larger ash particles, pointing to aerosol originating from an uncommon transport towards the north of plumes from Mount Etna eruption.

Starting from the measured aerosol optical properties, the particle size distribution was retrieved from lidar data using a novel inversion approach. The algorithm was validated with measured data in the two observed layers and the obtained particles size distributions resulted very different. The Saharan dust plume shows a more elevated particle concentration in the coarse mode fraction, due to a larger mean size expected for the Saharan dust aerosol, with finer particles in the accumulation mode possibly related to local, urban aerosol contributions or very fine dust. The size distribution linked to volcanic plume shows a predominance of the fine particles mode due to the deposition of larger volcanic ash particles during the transport from the volcanic source.

The obtained results demonstrate how the combination of a multi-parametric Lidar with other instruments allows gaining a clear classification of the atmospheric aerosol, even for multilayered atmospheric conditions. The new information provided by vertically-resolved lidar inversion of aerosol microphysics proved crucial towards the characterization of this event. These results are very promising and the extension of the method to other aerosol typologies will be the subject of future studies.

Acknowledgments:

The research leading to these results has received funding from the European Union's Horizon 2020 Framework Program for Research and Innovation (grant agreement no. 654109 – ACTRIS-2 Aerosols, Clouds, and Trace Gases Research InfraStructure). The authors gratefully acknowledge the NOAA Air Resource Laboratory (ARL) for provision the HYSPLIT transport and dispersion

model and /or READY website used in this publication. Data and/or from the BSC- DREAM8b (Dust Regional Atmospheric Model) model were operated by the Barcelona Supercomputing Center (http://www.bsc.es/ess/bsc-dust-daily-forecast/). The ECMWF is acknowledged for providing the meteorological analyses used for the FLEXPART simulations.
The authors thank ALA Advanced Lidar Applications s.r.l. for providing the PAPRICA software for the lidar microphysical properties retrieval.
The authors thank M. Prestifilippo for keeping the service of the volcanic ash dispersal and fallout forecasts at INGV-OE also in the frame of the VAMOS SEGURO project (http://www.vamosseguro.eu/) and S. Corradini, D. Stelitano and L. Gurreri for providing input emissions for the FLEXPART SO_2 dispersion modelling. Finally, the authors thank B. Behncke for providing the photo of the Etna's eruption column used in the graphical abstract.

References:

Ansmann, A., Riebesell, M., and Weitkamp, C., 1990. Measurement of atmospheric aerosol extinction profiles with a Raman lidar. Opt. Lett. 15, 746–748.doi:10.1364/OL.15.000746.

Ansmann, A., Riebesell, M., Wandinger, U., Weitkamp, C., Voss, E., Lahmann, W., Michaelis, W., 1992, Combined raman elastic-backscatter LIDAR for vertical profiling of moisture, aerosol extinction, backscatter, and LIDAR ratio. App. Phys. B., 55:18. doi:10.1007/BF00348608.

Azzopardi, F., Ellul, R., Prestifilippo, M., Scollo, S., and Coltelli, M., 2013. The effect on Etna volcanic ash clouds on the Maltese Islands. J. Volcanol. Geotherm. Res. 260, 13–26. https://doi.org/10.1016/j.jvolgeores.2013.04.019 .

Baars, H., Ansmann, A., Ohneiser, K., Haarig, M., Engelmann, R., Althausen, D., Hanssen, I., Gausa, M., Pietruczuk, A., Szkop, A., Stachlewska, I. S., Wang, D., Reichardt, J., Skupin, A., Mattis, I., Trickl, T., Vogelmann, H., Navas-Guzmán, F., Haefele, A., Acheson, K., Ruth, A. A., Tatarov, B., Müller, D., Hu, Q., Podvin, T., Goloub, P., Veselovskii, I., Pietras, C., Haeffelin, M., Fréville, P., Sicard, M., Comerón, A., Fernández García, A. J., Molero Menéndez, F., Córdoba-Jabonero, C., Guerrero-Rascado, J. L., Alados-Arboledas, L., Bortoli, D., Costa, M. J., Dionisi, D., Liberti, G. L., Wang, X., Sannino, A., Papagiannopoulos, N., Boselli, A., Mona, L., D'Amico, G., Romano, S., Perrone, M. R., Belegante, L., Nicolae, D., Grigorov, I., Gialitaki, A., Amiridis, V., Soupiona, O., Papayannis, A., Mamouri, R.-E., Nisantzi, A., Heese, B., Hofer, J., Schechner, Y. Y., Wandinger, U., and Pappalardo, G., 2019. The unprecedented 2017–2018 stratospheric smoke event: decay phase and aerosol properties observed with the EARLINET, Atmos. Chem. Phys. 19, 15183–15198, https://doi.org/10.5194/acp-19-15183-2019.

Bègue, N., Shikwambana, L., Bencherif, H., Pallotta, J., Sivakumar, V., Wolfram, E., Mbatha, N., Orte, F., Du Preez, D. J., Ranaivombola, M., Piketh, S., and Formenti, P., 2020. Statistical analysis of the long-range transport of the 2015 Calbuco volcanic plume from ground-based and space-borne observations, Ann. Geophys., 38, 395–420, https://doi.org/10.5194/angeo-38-395-2020.

Biele, J., Beyerle, G. and Baumgarten, G., 2000. Polarization lidar: corrections of instrumental effects. Opt. Express, 7,427–435.doi:10.1364/OE.7.000427.

Böckmann, C.,Wandinger, U., Ansmann, A., Bösenberg, J., Amiridis, V., Boselli, A., Delaval, A., Tomasi, F.D., Frioud, M., Hågård, A., Iarlori, M., Komguem, L., Kreipl, S., Larchevêque, G., Matthias, V., Papayannis, A., Pappalardo G., Rochadenbosch, F., Rodrigues, J., Schneider, J., Shcherbakov, V., and Wiegner, M., 2004. Aerosol lidar intercomparison in the frame of EARLINET. Part II: Aerosol backscatter algorithms. Appl. Opt. 43,Issue4, 977-989, doi: 10.1364/ao.43.000977.

Bockmann, C., Miranova, C., Muller, D., Scheidenbach, L., and Nessler, R., 2005. Microphysical aerosol parameters from multiwavelength lidar. J. Opt. Soc. Am. 22, 518–528, doi:10.1364/JOSAA.22.000518.

Boselli, A., Sannino, A., D'Emilio, M., Wang, X., Amoruso, S., 2021. Aerosol characterization during the summer 2017 huge fire event on mount Vesuvius (Italy) by remote sensing and in situ observations. Remote Sens. Volume 13, Issue 10, https://doi.org/10.3390/rs13102001.

Burton, S. P., Chemyakin, E., Liu, X., Knobelspiesse, K., Stamnes, S., Sawamura, P., Moore, R. H., Hostetler, C. A., and Ferrare, R. A., 2016. Information content and sensitivity of the $3\beta + 2\alpha$ lidar measurement system for aerosol microphysical retrievals. Atmos. Meas. Tech. 9, 5555–5574, https://doi.org/10.5194/amt-9-5555-2016.

Chemyakin, E., Burton, S., Kolgotin, A., Müller, D., Hostetler, C., and Ferrare, R., 2016. Retrieval of aerosol parameters from multiwavelength lidar: investigation of the underlying inverse mathematical problem. Appl. Opt. 55, 2188–2202, doi:10.1364/AO.55.002188.

Di Iorio, T., di Sarra, A., Sferlazzo, D. M., Cacciani, M., Meloni, D., Monteleone, F., Fua` D. and Fiocco, G., 2009. Seasonal evolution of the tropospheric aerosol vertical profile in the central Mediterranean and role of desert dust. J. Geophys. Res. 114, D02201, doi:10.1029/2008JD010593.

Dubovik, O. and King, M.D., 2000. A flexible inversion algorithm for the retrieval of aerosol optical properties from sun and sky radiance measurements. J. Geophys. Res. 105: 20,673–20,696. doi:10.1029/2000JD900282.

Dubovik, O., Smirnov, A., Holben, B. N., King, M. D., Kauf-man, Y. J., Eck, T. F., and Slutsker, I., 2000. Accuracy assessments of aerosol optical properties retrieved from AERONET sun and sky-radiance measurements. J. Geophys. Res., 105, 9791–9806.

Fernald, F. G., 1984. Analysis of the atmospheric lidar observations; some comments. Appl. Opt. 23, 652–653.doi:10.1364/AO.23.000652.

Freudenthaler,V., Esselborn, M., Wiegner, M., Heese, B., Tesche, M., Ansmann, A., Muller, D., Althausen, D., Wirth, M., Fix, A., Ehret, G., Knippertz, P., Toledano, C., Gasteiger, J., Garhammer, M., Seefeldner, M., 2009. Depolarization ratio profiling at several wavelengths in pure Saharan dust during SAMUM 2006. Tellus, 61B, 165–179. Doi: 10.1111/j.16000889.2008.00396.x.

Ghan, S. J., Liu, X., Easter Jr. R. C., Zaveri, R. A., Rasch, P. J., Yoon, J. H., Eaton B., 2012. Toward a minimal representation of aerosols in climate models: Comparative decomposition of aerosol direct, semidirect, and indirect radiative forcing, J. Clim., 25, 6461–6476, doi:10.1175/JCLI-D-11-00650.1.1.

Giles, D. M., Sinyuk, A., Sorokin, M. G., Schafer, J. S., Smirnov, A., Slutsker, I., Eck, T. F., Holben, B. N., Lewis, J. R., Campbell, J. R., Welton, E. J., Korkin, S. V., Lyapustin, A. I., 2019. Advancements in the Aerosol Robotic Network (AERONET) Version 3 database – automated near-real-time quality control algorithm with improved cloud screening for Sun photometer aerosol optical depth (AOD) measurements. Atmos. Meas.Tech. 12: 169–209. https://doi.org/10.5194/amt-12-169-2019.

Hatzianastassiou, N., Gkikas, A., Mihalopoulos, N., Torres, O., and Katsoulis B. D., 2009. Natural versus anthropogenic aerosols in the eastern Mediterranean basin derived from multiyear TOMS and MODIS satellite data, J. Geophys. Res.114, D24202,doi:10.1029/2009JD011982.

Holben, B.N., Eck, T.F., Slutsker, I., Tanré, D., Buis, J.P., Setzer, A., Vermote, E., Reagan, J.A., Kaufman, Y.J., Nakajima, T., Lavenu, F., Jankowiak, I., Smirnov, A., 1998. AERONET-a federated instrument network and data archive for aerosol characterization. Remote Sens. Environ. 66, 1–16.

Holben, B.N., Tanré, D., Smirnov, A., Eck, T.F., Slutsker, I., Abuhassan, N., Newcomb, W.W., Schafer, J., Chatenet, B., Lavenue, F., Kaufman, Y.J., Vande Castle, J., Setzer, A., Markham, B., Clark, D., Frouin, R., Halthore, R., Karnieli, A., O'Neill, N.T., Pietras, C., Pinker, R.T., Voss, K., Zibordi, G., 2001. An emerging ground-based aerosol climatology: aerosol optical depth from AERONET. J. Geophys. Res. 106: 12,067–12,097. doi:10.1029/ 2001JD900014.

Khedidji, S., Müller, K., Rabhi, L., Spindler, G., Fomba, K.W., Pinxteren, D.V., Yassaa, N. and Herrmann, H., 2020. Chemical Characterization of Marine Aerosols in a South Mediterranean Coastal Area Located in Bou Ismaïl, Algeria. Aerosol Air Qual. Res. 20: 2448–2473. https://doi.org/10.4209/aaqr.2019.09.0458.

Klekociuk, A.R.; Ottaway, D.J.; MacKinnon, A.D.; Reid, I.M.; Twigger, L.V.; Alexander, S.P. Australian Lidar Measurements of Aerosol Layers Associated with the 2015 Calbuco Eruption. Atmosphere 2020, 11, 124. https://doi.org/10.3390/atmos11020124.

Klett, J.D. (1981). Stable analytical inversion solution for processing lidar returns. Appl. Opt. 20, 211–220.doi:10.1364/AO.20.000211.

Lakkala, K., Kujanpää, J., Brogniez, C., Henriot, N., Arola, A., Aun, M., Auriol, F., Bais, A. F., Bernhard, G., De Bock, V., Catalfamo, M., Deroo, C., Diémoz, H., Egli, L., Forestier, J.-B., Fountoulakis, I., Garane, K., Garcia, R. D., Gröbner, J., Hassinen, S., Heikkilä, A., Henderson, S., Hülsen, G., Johnsen, B., Kalakoski, N., Karanikolas, A., Karppinen, T., Lamy, K., León-Luis, S. F., Lindfors, A. V., Metzger, J.-M., Minvielle, F., Muskatel, H. B., Portafaix, T., Redondas, A., Sanchez, R., Siani, A. M., Svendby, T., and Tamminen, J., 2020. Validation of the TROPOspheric Monitoring Instrument (TROPOMI) surface UV radiation product. Atmos. Meas. Tech. 13, 6999–7024, https://doi.org/10.5194/amt-13-6999-2020.

Lelieveld, J., Berresheim, H., Borrmann, S., Crutzen, P. J., Dentener, J. Fischer, H. Feichter, J., Flatau, J., Heland, J., Holzinger, R., Korrmann, R., Lawrence, M. G., Levin, Z., Markowicz, K., M., Mihalopoulos, N., Minikin, A., Ramanathan, V., de Reus, M.1 Roelofs, G.J., Scheeren, H.A., Sciare, J., Schlager, H.,Schultz, M.,Siegmund, P., Steil, B., Stephanou, E.G., Stier, P., Traub, M., Warneke, C., Williams, J., Ziereis, H., 2002. Global Air Pollution Crossroads over the Mediterranean. Science. Vol 298, Issue 5594, 794-799, doi: 10.1126/science.1075457.

Lopes, J.S.F., Silva, J.J., Antuña Marrero, J.C., Taha, G., Landulfo, E., 2019. Synergetic Aerosol Layer Observation After the 2015 Calbuco Volcanic Eruption Event. Remote Sens. 11, 195. https://doi.org/10.3390/rs11020195

Mallet, M. D., D'Anna, B., Même, A., Bove, M. C., Cassola, F., Pace, G., Desboeufs, K., Di Biagio, C., Doussin, J.-F., Maille, M., Massabò, D., Sciare, J., Zapf, P., di Sarra, A. G. and Formenti, P., 2019. Summertime surface PM1 aerosol composition and size by source region at the Lampedusa island in the central Mediterranean Sea. Atmos. Chem. Phys. 19, 11123–11142, https://doi.org/10.5194/acp-19-11123-2019, 2019.

Mattis, I., Seifert, P., Muller, D., Tesche, M., Hiebsch, A., Kanitz, T., Schmidt, J., Finger, F., Wandinger, U., and Ansmann, A., 2010. Volcanic aerosol layers observed with multiwavelength Raman lidar over Central Europe in 2008–2009. J. Geophys. Res., 115, D00L04, doi:10.1029/2009JD013472, 2010.

McLean, W. G., Fu, G., Burton, S. P., and Hasekamp, O. P., 2021. Retrieval of aerosol microphysical properties from atmospheric lidar sounding: an investigation using synthetic measurements and data from the ACEPOL campaign. Atmos. Meas. Tech., 14, 4755–4771, 2021https://doi.org/10.5194/amt-14-4755-2021.

Michaelides, S., Karacostas, T., Sánchez, J.L., Retalis, A., Pytharoulis, I., Homar, V., Romero, R., Zanis, P., Giannakopoulos, C., Bühl, J., Ansmann, A., Merino, A., Melcon, P., Konstantinos Lagouvardos, K., Kotroni, V., Bruggeman, A., López-Moreno, J.I., Berthet, C., Katragkou, E., Tymvios, F., Hadjimitsis, D.G., Mamouri, R.-E., Nisantzi, A., 2018. Reviews and perspectives of high impact atmospheric processes in the Mediterranean. Atmos. Res. 208, 4-44. https://doi.org/10.1016/j.atmosres.2017.11.022.

Mona, L., Amodeo, A., D'Amico, G., Giunta, A., Madonna, F., and Pappalardo, G., 2012. Multi-wavelength Raman lidar observations of the Eyjafjallajökull volcanic cloud over Potenza, southern Italy, Atmos. Chem. Phys., 12, 2229–2244, https://doi.org/10.5194/acp-12-2229-2012.

Müller, D., Wandinger, U. and Ansmann, A., 1999. Microphysical particle parameters from extinction and backscatter lidar data by inversion with regularization: theory. Appl. Opt. 38, 2346–2357, doi:10.1364/AO.38.002346.

Müller, D., Ansmann, A., Mattis, I., Tesche, M., Wandinger, U., Althausen, D. and Pisani G., 2007. Aerosol-type-dependent lidar ratios observed with Raman lidar. J. Geophys. Res. 112, D16202, doi:10.1029/2006JD008292.

Noh, Y.M., Shin, D.H., Müller, D., 2017. Variation of the vertical distribution of Nabro volcano aerosol layers in the stratosphere observed by LIDAR, Atmos. Environ. 154, 1-8, https://doi.org/10.1016/j.atmosenv.2017.01.033.

Pace, G., Meloni, D. and di Sarra A., 2005. Forest fire aerosol over the Mediterranean basin during summer 2003. J. Geophys. Res. 110, D21202, doi:10.1029/2005JD005986.

Pandolfi, M., Cusack, M., Alastuey, A. and Querol, X., 2011. Variability of aerosol optical properties in the Western Mediterranean Basin. Atmos. Chem. Phys. 11, 8189–8203, https://doi.org/10.5194/acp-11-8189-2011.

Papayannis, A., Mamouri, R. E., Amiridis, V., Giannakaki, E., Veselovskii, I., Kokkalis, P., Tsaknakis, G., Balis, D., Kristiansen, N. I., Stohl, A., Korenskiy, M., Allakhverdiev, K., Huseyinoglu, M. F., and Baykara, T., 2011. Optical properties and vertical extension of aged ash layers over the Eastern Mediterranean as observed by Raman lidars during the Eyjafjallajokull eruption in May 2010. Atmos. Environ., 48, 56–65, doi:10.1016/j.atmosenv.2011.08.037.

Papayannis, A., Mamouri, R. E., Amiridis, V., Remoundaki, E., Tsaknakis, G., Kokkalis, P., Veselovskii, I., Kolgotin, A., Nenes, A., and Fountoukis, C., 2012. Optical-microphysical properties of Saharan dust aerosols and composition relationship using a multi-wavelength Raman lidar, in situ sensors and modelling: a case study analysis. Atmos. Chem. Phys. 12, 4011–4032, https://doi.org/10.5194/acp-12-4011-2012.

Papanikolaou, C.A. , Giannakaki, E., Papayannis, A., Mylonaki, M., Soupiona, O., 2020. Canadian Biomass Burning Aerosol Properties Modification during a Long-Ranged Event on August 2018. Sensors, 20, 5442; doi:10.3390/s20185442.

Pappalardo, G., Amodeo, A., Mona, L., Pandolfi, M., Pergola, N. and Cuomo V., 2004. Raman lidar observations of aerosol emitted during the 2002 Etna eruption. Geophys. Res. Lett. 31, doi:10.1029/2003GL019073.

Pappalardo, G., Amodeo, A., Pandolfi, M., Wandinger, U., Ansmann, A., Bösenberg, J., Matthias, V., Amiridis, V., De Tomasi, F., Frioud, M., Iarlori, M., Komguem, L., Papayannis, A., Rocadenbosch, F. and Wang X., 2004. Aerosol lidar intercomparison in the framework of the EARLINET project. 3. Raman lidar algorithm for aerosol extinction, backscatter, and lidar ratio. Appl. Opt. Vol. 43, No. 28, https://doi.org/10.1364/AO.43.005370.

Pappalardo, G., Mona, L., D'Amico, G., Wandinger, U., Adam, M., Amodeo, A., Ansmann, A., Apituley, A., Alados Arboledas, L., Balis, D., Boselli, A., Bravo-Aranda, J. A., Chaikovsky, A., Comeron, A., Cuesta, J., De Tomasi, F., Freudenthaler, V., Gausa, M., Giannakaki, E., Giehl, H., Giunta, A., Grigorov, I., Groß, S., Haeffelin, M., Hiebsch, A., Iarlori, M., Lange, D., Linné, H., Madonna, F., Mattis, I., Mamouri, R.-E., McAuliffe, M. A. P., Mitev, V., Molero, F., Navas-Guzman, F., Nicolae, D., Papayannis, A., Perrone, M. R., Pietras, C., Pietruczuk, A., Pisani, G., Preißler, J., Pujadas, M., Rizi, V., Ruth, A. A., Schmidt, J., Schnell, F., Seifert, P., Serikov, I., Sicard, M., Simeonov, V., Spinelli, N., Stebel, K., Tesche, M., Trickl, T., Wang, X., Wagner, F., Wiegner, M., and Wilson, K. M., 2013. Four-dimensional distribution of the 2010 Eyjafjallajökull volcanic cloud over Europe observed by EARLINET, Atmos. Chem. Phys., 13, 4429–4450, https://doi.org/10.5194/acp-13-4429-2013.

Pappalardo, G., Amodeo, A., Apituley, A., Comeron, A., Freudenthaler, V., Linné, H., Ansmann, A., Bösenberg, J., D'Amico, G., Mattis, I., Mona, L., Wandinger, U., Amiridis, V., Alados-Arboledas, L., Nicolae, D. and Wiegner, M., 2014. EARLINET: towards an advanced sustainable European aerosol lidar network. Atmos. Meas. Tech. 7, 2389-2409, https://doi.org/10.5194/amt-7-2389-2014.

Pappalardo, G., 2018. ACTRIS Aerosol, Clouds and Trace Gases Research Infrastructure. EPJ Web Conference, 176. https://doi.org/10.1051/epjconf/201817609004.

Pérez-Ramírez, D., Whiteman, D. N., Veselovskii, I., Korenski, M., Colarco, P. R., and da Silva, A. M.,2020. Optimized profile retrievals of aerosol microphysical properties from simulated spaceborne multiwavelength lidar. J. Quant. Spectrosc. Radiat. Transf. 246, 106 932 https://doi.org/10.1016/j.jqsrt.2020.106932.

Perrone, M., Becagli, S., Orza, J. G., Vecchi, R., Dinoi, A., Udisti, R., and Cabello, M., 2013. The impact of long-range-transport on PM1 and PM2.5 at a Central Mediterranean site. Atmos. Environ. 71, 176–186, doi:10.1016/j.atmosenv.2013.02.006.

Perrone, M.R., Burlizzi, P., 2016. Mediterranean aerosol typing by integrating three-wavelength lidar and sun photometer measurements. Environ. Sci. Pollut. Res. 23, 14123–14146,. https://doi.org/10.1007/s11356-016-6575-7.

Pisani, G., Boselli, A., Spinelli, N., Wang, X., 2011. Characterization of Saharan dust layers over Naples (Italy) during 2000-2003 EARLINET project. Atmos. Res. 102, 3, 286-299, doi: 10.1016/j.atmosres.2011.07.012.

Pisso, I., Sollum, E., Grythe, H., Kristiansen, N. I., Cassiani, M., Eckhardt, S., Arnold, D., Morton, D., Thompson, R. L., Groot Zwaaftink, C. D., Evangeliou, N., Sodemann, H., Haimberger, L., Henne, S., Brunner, D., Burkhart, J. F., Fouilloux, A., Brioude, J., Philipp, A., Seibert, P., and

Stohl, A., 2019. The Lagrangian particle dispersion model FLEXPART version 10.4. Geosci. Model Dev. 12, 4955–4997, https://doi.org/10.5194/gmd-12-4955-2019.

Sawamura, P., Vernier, J.P., Barnes, J.E., Berkoff, T.A., Welton, E.J., Alados-Arboledas, L., Navas-Guzmán, F., Pappalardo, G., Mona, L., Madonna, F., Lange, D., Sicard, M., Godin-Beekmann, S., Payen, G., Wang, Z., Hu, S., Tripathi, N., Cordoba-Jabonero, C., Hoff, R.M.,2012. Stratospheric AOD after the 2011 eruption of Nabro volcano measured by lidars over the Northern Hemisphere. Environ. Res. Lett. 7, 034013, https://doi.org/10.1088/1748-9326/7/3/034013.

Scollo, S., Kahn, R. A., Nelson, D. L., Coltelli, M., Diner, D. J., Garay M. J. and Realmuto V. J., 2012. MISR observations of Etna volcanic plumes, J. Geophys. Res. 117, D06210, doi:10.1029/2011JD016625.

Sellitto, P., di Sarra, A., Corradini, S., Boichu, M., Herbin, H., Dubuisson, P., Seze, G., Meloni, D., Monteleone, F., Merucci, L., Rusalem, J., Salerno, G., Briole, P., Legras, B., 2016. Synergistic use of Lagrangian dispersion and radiative transfer modelling with satellite and surface remote sensing measurements for the investigation of volcanic plumes: the Mount Etna eruption of 25–27 October 2013. Atmos. Chem. Phys. 16, 6841-6861, https://doi.org/10.5194/acp-16-6841-2016.

Sellitto, P., Zanetel, C., di Sarra, A., Salerno, G., Tapparo, A., Meloni, D., Pace, G., Caltabiano, T., Briole, P., Legras, B., 2017. The impact of Mount Etna sulfur emissions on the atmospheric composition and aerosol properties in the central Mediterranean: A statistical analysis over the period 2000-2013 based on observations and Lagrangian modelling. Atmos. Environ. 148, 77-88, https://doi.org/10.1016/j.atmosenv.2016.10.032.

Sellitto, P., Salerno, G., La Spina, A., Caltabiano, T., Scollo, S., Boselli, A., Leto, G., Zanmar Sanchez, R., Crumeyrolle, S., Hanoune, B., Briole, P., 2020. Small-scale volcanic aerosols variability, processes and direct radiative impact at Mount Etna during the EPL-RADIO campaigns, Scientific Reports, 10, 15224, https://doi.org/10.1038/s41598-020-71635-1.

Sellitto, P., Salerno G., Corradini, S., Xueref-Remy, I., Riandet, A., Bellon, C., M Khaykin, S., Ancellet, G., Lolli, S., J Welton, E., Boselli, A., Sannino, A., Cuesta, J., Guermazi, H., Eremenko, M., Merucci, L., Stelitano, D., Guerrieri L., Legras, B., 2021. Volcanic Emissions, Plume Dispersion and Downwind Radiative Impacts following Mount Etna Series of Eruptions of 21-26 February 2021, Under submission to J. Geophys. Res. https://doi.org/10.1002/essoar.10508145.1.

Sorrentino, A., Sannino, A., Spinelli, N., Piana, M., Boselli, A., Tontodonato, V., Castellano, P., and Wang, X., 2021. Retrieving the atmospheric number size distribution from lidar data. Atmos. Meas. Tech. Discussion, https://doi.org/10.5194/amt-2021-152.

Soupiona, O., Samaras, S., Ortiz-Amezcua, P., Böckmann, C., Papayannis, A., Moreira, G.A., Benavent-Oltra, J.A., Guerrero-Rascado, J.L., Bedoya-Velásquez, A.E., Olmo, F.J., Román, R., Kokkalis, P., Mylonaki, M., Alados-Arboledas, L., Papanikolaou, C.A., Foskinis, R., 2019. Retrieval of optical and microphysical properties of transported Saharan dust over Athens and Granada based on multi-wavelength Raman lidar measurements: Study of the mixing processes. Atmos. Environ. 214, 116824, ISSN 1352-2310, doi:.1016/j.atmosenv.2019.116824.

Soupiona, O., Papayannis, A., Kokkalis, P., Foskinis, R., Sánchez Hernández, G., Ortiz-Amezcua, P., Mylonaki, M., Papanikolaou, C.A., Papagiannopoulos, N., Samaras, S., Groß, S., Mamouri, R.-E., Alados-Arboledas, L., Amodeo, A., and Psiloglou, B., 2020. EARLINET observations of Saharan dust intrusions over the northern Mediterranean region (2014–2017): properties and impact on radiative forcing. Atmos. Chem. Phys. 20, 15147–15166, https://doi.org/10.5194/acp-20-15147-2020.

Sulpizio, R., Zanchetta, G., Caron, B., Dellino, P., Mele, D., Giaccio, B., Insinga, D., Paterne, M., Siani, G., Costa, A., Macedonio, G., Santacroce, R., 2014. Volcanic ash hazard in the Central Mediterranean assessed from geological data. Bull. Volcanol. 76, 866, https://doi.org/10.1007/s00445-014-0866-y.

Thomas, W., Erbertseder, T., Ruppert, T., van Roozendael, M., Verdebout, J., Balis, D., Meleti, C. and Zerefos C., 2005. On the retrieval of volcanicsulfur dioxide emissions from GOME backscatter measurements. J. .Atmos. Chem. 50, 295 – 320.

Valenzuela, A., Olmo, F. J., Lyamani, H., Granados-Muñoz, M. J., Antón, M., Guerrero-Rascado, J. L., Quirantes, A., Toledano, C., Perez-Ramírez, D. and Alados-Arboledas L., 2014. Aerosol transport over the western Mediterranean basin: Evidence of the contribution of fine particles to desert dust plumes over Alborán Island. J. Geophys. Res. Atmos. 119,14,028–14,044, doi:10.1002/2014JD022044.

Vaughan, G., Wareing, D., and Ricketts, H., 2021. Measurement Report: Lidar measurements of stratospheric aerosol following the 2019 Raikoke and Ulawun volcanic eruptions, Atmos. Chem. Phys., 21, 5597–5604, https://doi.org/10.5194/acp-21-5597-2021.

Veefkind, J. P., Aben, I., McMullan, K., Förster, H., de Vries, J., Otter, G., Claas, J., Eskes, H. J., de Haan, J. F., Kleipool, Q., van Weele, M., Hasekamp, O., Hoogeveen, R., Landgraf, J., Snel, R., Tol, P., Ingmann, P., Voors, R., Kruizinga, B., Vink, R., Visser, H., and Levelt, P. F., 2012. TROPOMI on the ESA Sentinel-5 Precursor: A GMES mission for global observations of the atmospheric composition for climate, air quality and ozone layer applications. Remote Sens. Environ. 120, 70–83, https://doi.org/10.1016/j.rse.2011.09.027.

Xu, X., Xie, L., Yang, X.,Wu, H., Cai, L., Qi, P., 2020. Aerosol optical properties at seven AERONET sites over Middle East and Eastern Mediterranean Sea. Atmos. Environ. 243, 117884. ttps://doi.org/10.1016/j.atmosenv.2020.117884.

Ren-Jian, Z., Kin-Fai, H., Zhen-Xing, S. (2012), The Role of Aerosol in Climate Change, the Environment, and Human Health. Atmos. Oceanic Sci. Lett. 5:2, 156-161, doi: 10.1080/16742834.2012.11446983.

Zhang, B. W., 2020. The Effect of Aerosols to Climate Change and Society. J. Geosci. Environ. Prot. 8, 55-78. https://doi.org/10.4236/gep.2020.88006.

Figure and Table Captions

Fig.1: Left panels: Time variability of the Range Corrected lidar Signal (RCS) (a) and aerosol depolarization (δ) (b) retrieved on February 25th, 2021 from 08:29 to16:42 UTC. The spatial and temporal resolutions are 15 m and 60 s, respectively. Right panels: lidar profiles of aerosol backscattering (β), linear depolarization (δ) and extinction (α) derived from observations carried out from 16:12 to 16:42.

Fig.2: BSC DREAMS and HYSPLIT NOAA Model outputs showing Dust Optical Depth at 550nm (a) and hair mass back-trajectories ending over the measurement area between 0.5 and 3 km of altitude (b), respectively.

Fig.3: Meteosat image of the volcanic plume (a), PUFF model simulations of its dispersion (b), TROPOMI satellite image (c) and FLEXPART model outputs reporting the time-variability and the vertical profile of the SO_2 mass concentration (d-e).

Fig. 4: Temporal variation of the Aerosol Optical Depth (AOD) (a) and Angstrom exponent (440/870) (b), measured at Naples on February 25th, 2021.

Fig. 5: Volume particle size distributions as derived from: (a) AERONET sunphotometer data; (b) lidar data in the range 700-9000 m, (c) lidar data in the range 700-3500 m, lidar data in the range 7000-8500 m.

Tab. 1: Methods with derived dataset and outcomes used in the paper.

Tab. 2: Averaged values of particle properties (LR, δ, BAE and EAE) for the two selected layers as derived from the lidar measurements.

Lidar	α (z), β (z), δ (z), LR, BAE, EAE, dV/dlnr
Sun-photometer	AOD, γ, SSA, dV/dlnr
HYSPLIT	Air masses back-trajectories
NMMB/BSC-Dust	Desert dust concentration
PUFF	Volcanic plume dispersion
FLEXPART	SO_2 mass concentration
TROPOMI	Total column SO_2
METEOSAT	Volcanic plume spatial distribution

Table 1

Range (m)	LR_{355}(sr)	LR_{532}(sr)	δ(%)	$BAE_{532/355}$	$EAE_{532/355}$
700-3500	31±2	38±6	24±5	1.06±0.02	1.5±2.0
7000-8500	77±14	74±40	10±6	1.94±0.39	2.6±1.7

Table 2

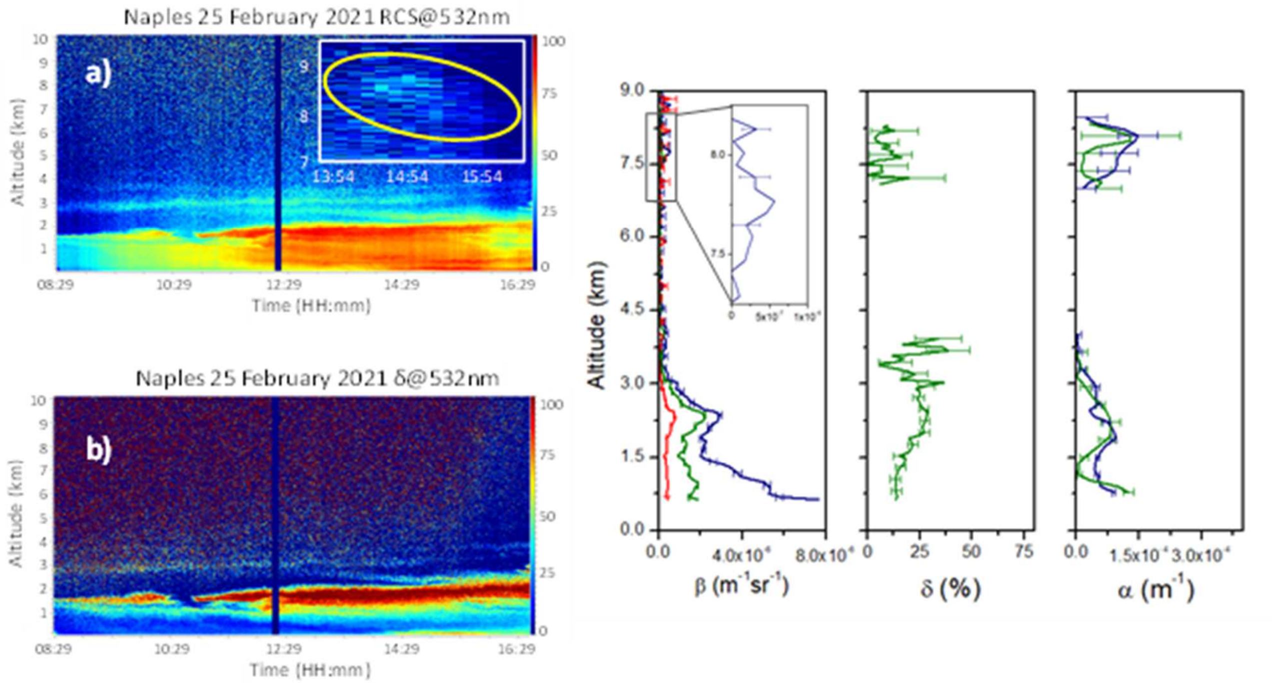

Naples 25 February 2021 RCS@532nm
a)
Altitude (km)
Time (HH:mm)
Naples 25 February 2021 δ@532nm
b)
Altitude (km)
Time (HH:mm)
Altitude (km)
β (m⁻¹sr⁻¹)
δ (%)
α (m⁻¹)

Figure 1

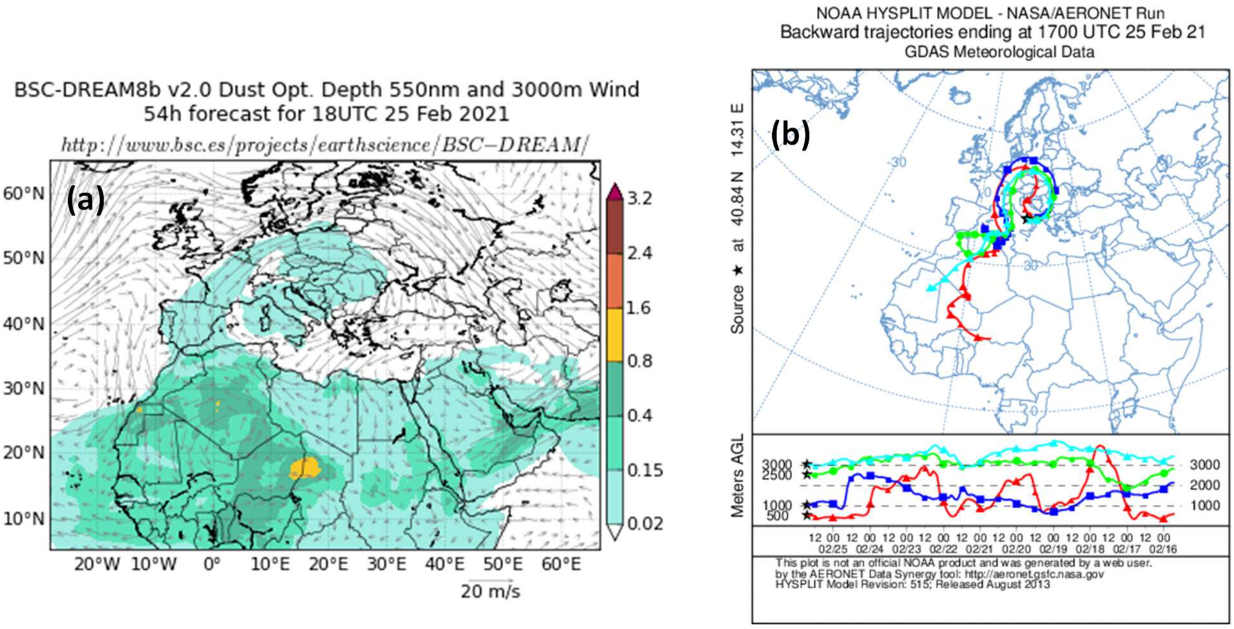

BSC-DREAM8b v2.0 Dust Opt. Depth 550nm and 3000m Wind
54h forecast for 18UTC 25 Feb 2021
http://www.bsc.es/projects/earthscience/BSC−DREAM/
(a)
60°N
50°N
40°N
30°N
20°N
10°N
20°W 10°W 0° 10°E 20°E 30°E 40°E 50°E 60°E
20 m/s
3.2
2.4
1.6
0.8
0.4
0.15
0.02
NOAA HYSPLIT MODEL - NASA/AERONET Run
Backward trajectories ending at 1700 UTC 25 Feb 21
GDAS Meteorological Data
(b)
Source ★ at 40.84 N 14.31 E
Meters AGL
3000
2500
1000
500
3000
2000
1000
12 00 12 00 12 00 12 00 12 00 12 00 12 00 12 00 12 00 12 00
02/25 02/24 02/23 02/22 02/21 02/20 02/19 02/18 02/17 02/16
This plot is not an official NOAA product and was generated by a web user.
by the AERONET Data Synergy tool: http://aeronet.gsfc.nasa.gov
HYSPLIT Model Revision: 515; Released August 2013

Figure 2

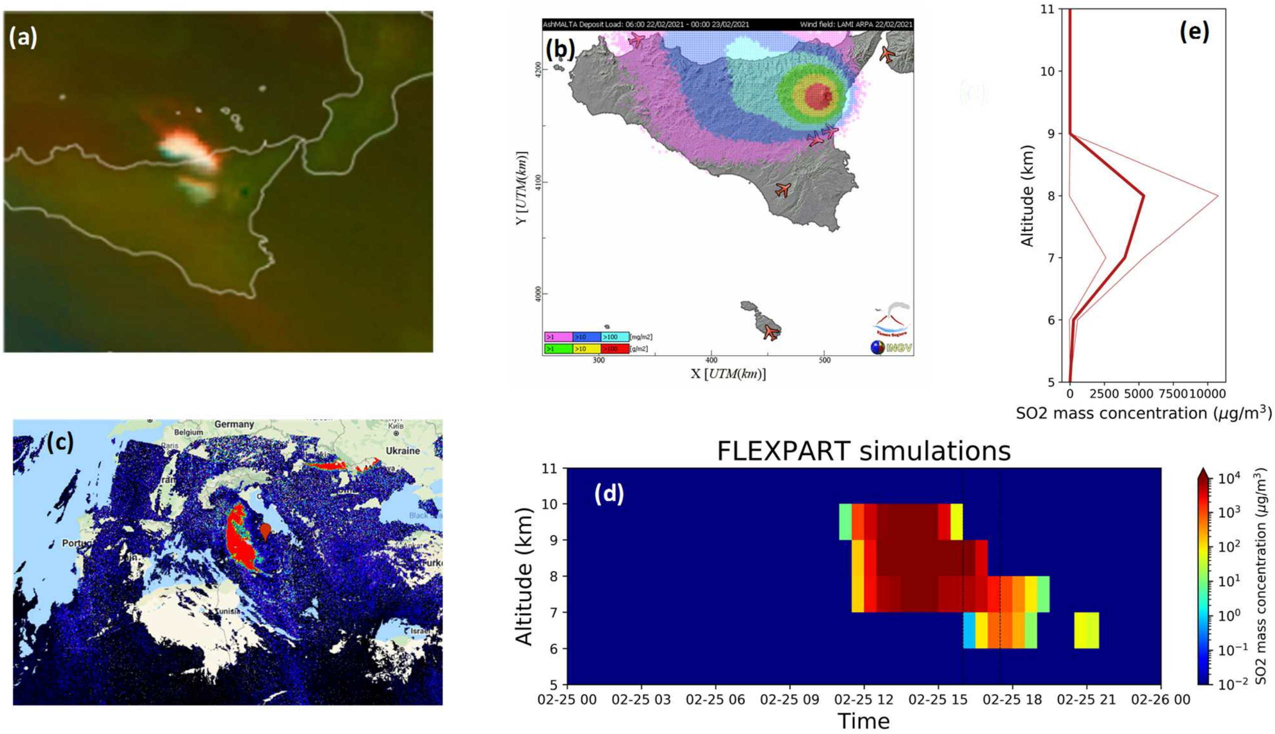
(a)
(b)
AshMALTA Deposit Load: 06:00 22/02/2021 - 00:00 23/02/2021
Wind field: LAMI ARPA 22/02/2021
Y [UTM(km)]
X [UTM(km)]
(e)
Altitude (km)
SO2 mass concentration (μg/m³)
(c)
Germany
Belgium
Ukraine
FLEXPART simulations
(d)
Altitude (km)
Time
02-25 00
02-25 03
02-25 06
02-25 09
02-25 12
02-25 15
02-25 18
02-25 21
02-26 00
SO2 mass concentration (μg/m³)

Figure 3

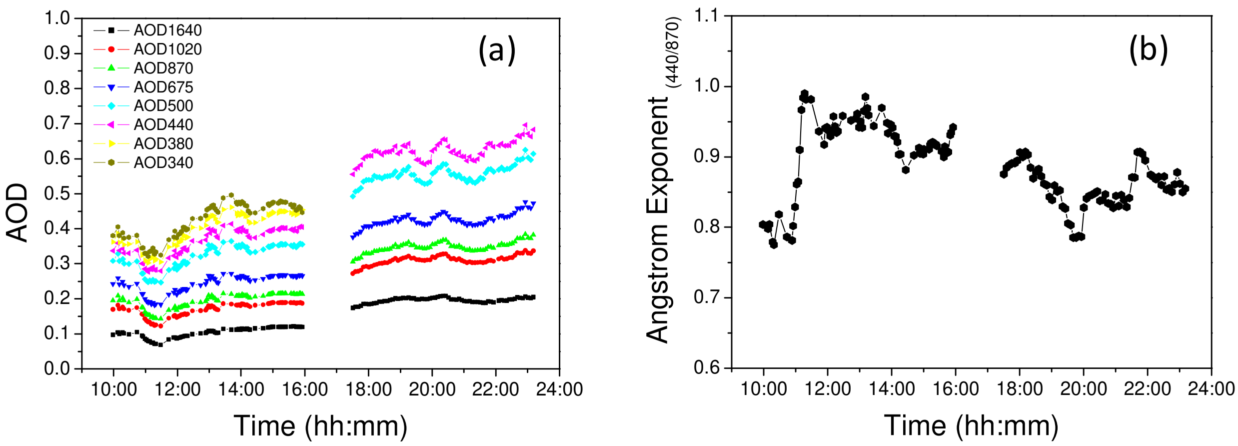
(a)
AOD1640
AOD1020
AOD870
AOD675
AOD500
AOD440
AOD380
AOD340
AOD
0.0
0.1
0.2
0.3
0.4
0.5
0.6
0.7
0.8
0.9
1.0
10:00
12:00
14:00
16:00
18:00
20:00
22:00
24:00
Time (hh:mm)
(b)
Angstrom Exponent (440/870)
0.6
0.7
0.8
0.9
1.0
1.1
10:00
12:00
14:00
16:00
18:00
20:00
22:00
24:00
Time (hh:mm)

Figure 4

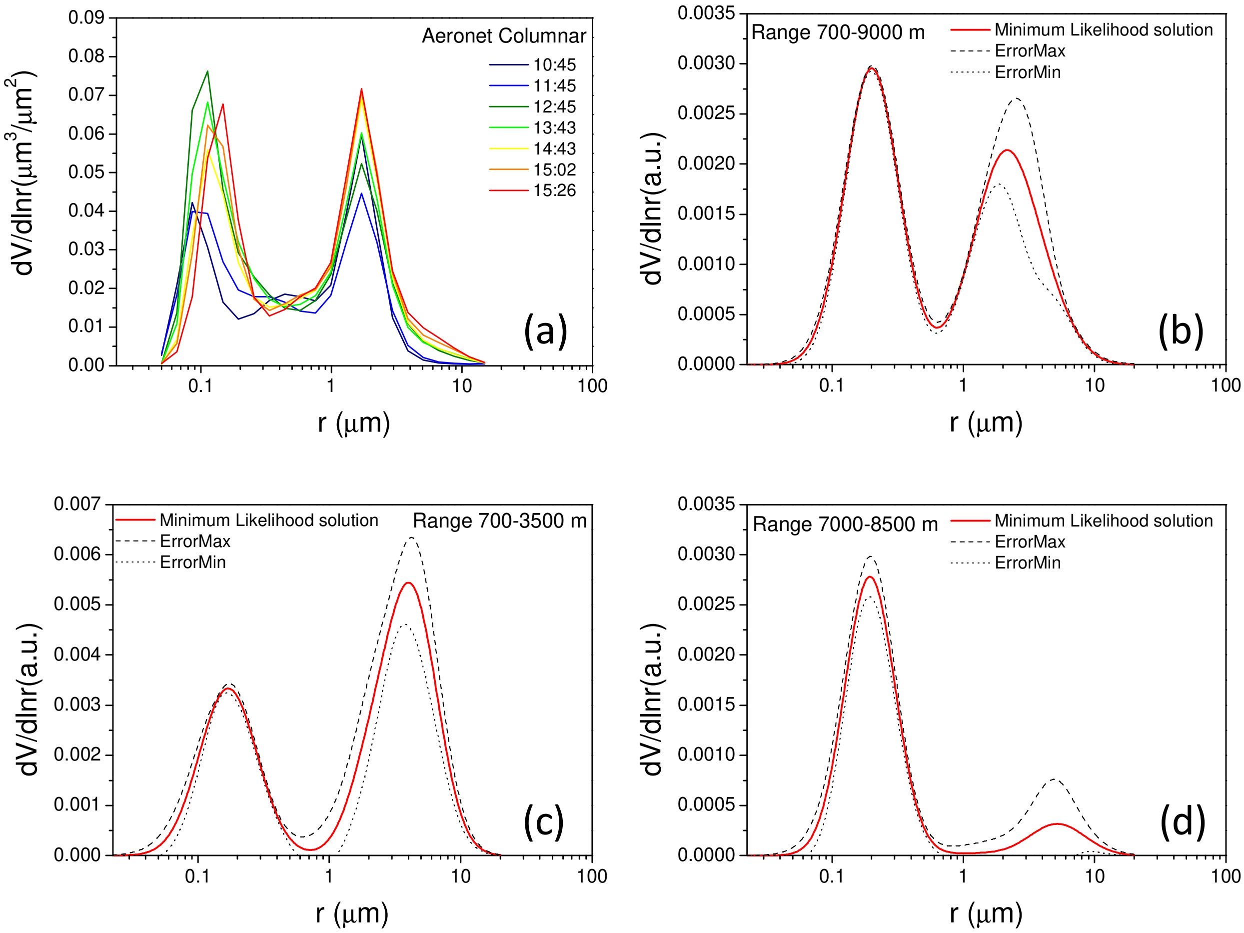
Aeronet Columnar
10:45
11:45
12:45
13:43
14:43
15:02
15:26
dV/dlnr(μm3/μm2)
r (μm)
(a)
Range 700-9000 m
Minimum Likelihood solution
ErrorMax
ErrorMin
dV/dlnr(a.u.)
r (μm)
(b)
Range 700-3500 m
Minimum Likelihood solution
ErrorMax
ErrorMin
dV/dlnr(a.u.)
r (μm)
(c)
Range 7000-8500 m
Minimum Likelihood solution
ErrorMax
ErrorMin
dV/dlnr(a.u.)
r (μm)
(d)

Figure 5

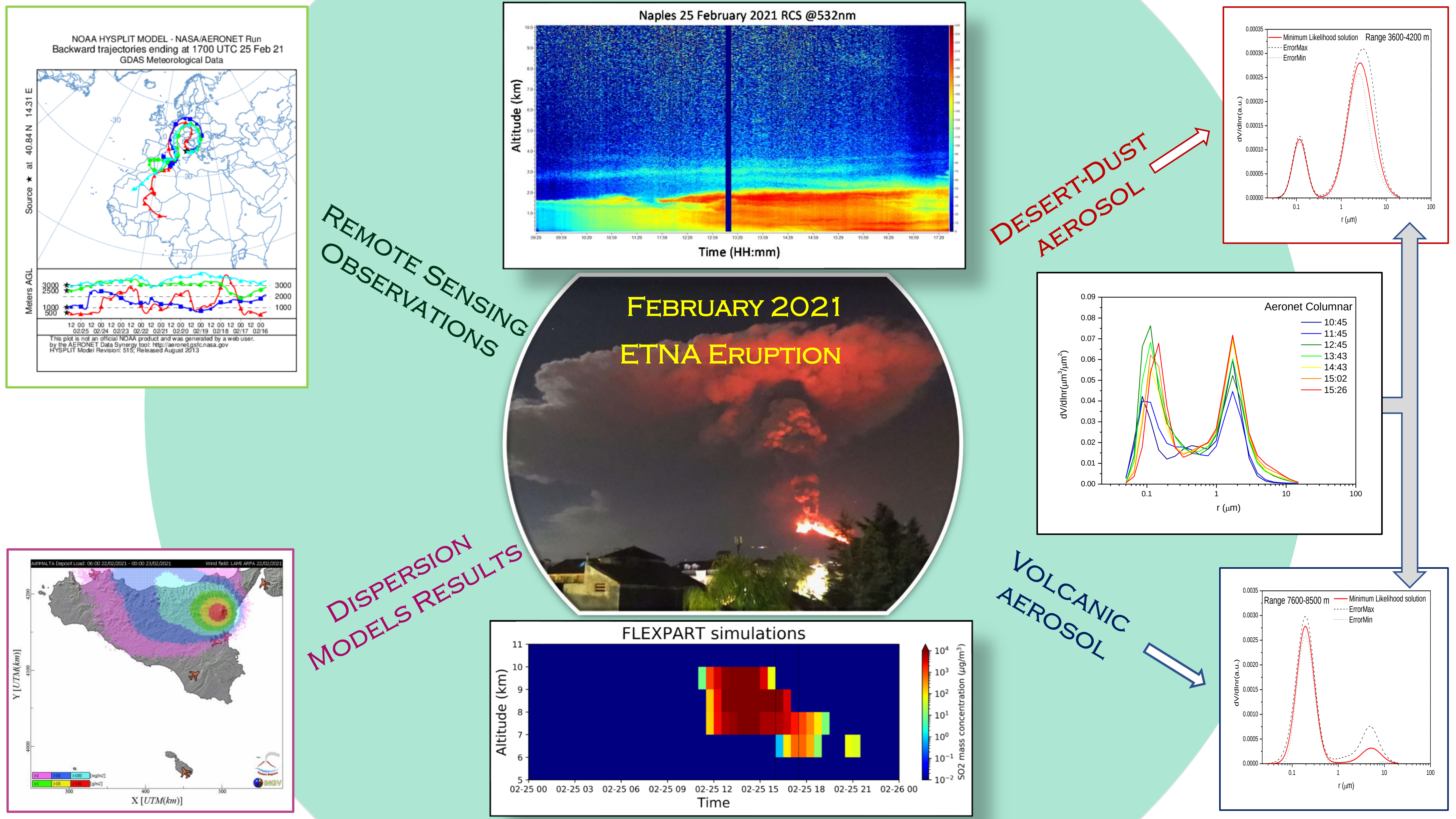

February 2021
ETNA Eruption
Remote Sensing Observations
Dispersion Models Results
Desert-Dust Aerosol
Volcanic Aerosol
NOAA HYSPLIT MODEL - NASA/AERONET Run
Backward trajectories ending at 1700 UTC 25 Feb 21
GDAS Meteorological Data
Source ★ at 40.84 N 14.31 E
Meters AGL
This plot is not an official NOAA product and was generated by a web user.
by the AERONET Data Synergy tool: http://aeronet.gsfc.nasa.gov
HYSPLIT Model Revision: 515; Released August 2013
Naples 25 February 2021 RCS @532nm
Altitude (km)
Time (HH:mm)
Minimum Likelihood solution
ErrorMax
ErrorMin
Range 3600-4200 m
dV/dlnr(a.u.)
r (μm)
Aeronet Columnar
10:45
11:45
12:45
13:43
14:43
15:02
15:26
dV/dlnr(μm³/μm²)
r (μm)
Range 7600-8500 m
Minimum Likelihood solution
ErrorMax
ErrorMin
dV/dlnr(a.u.)
r (μm)
FLEXPART simulations
Altitude (km)
Time
SO2 mass concentration (μg/m³)
02-25 00
02-25 03
02-25 06
02-25 09
02-25 12
02-25 15
02-25 18
02-25 21
02-26 00
Y [UTM(km)]
X [UTM(km)]
INGV